

# A Phase-Field Model for the Pinchoff of Liquid-Liquid Jets

Chang-Hun Kim\* and Seung-Ho Shin†

*Department of Computer Science, Korea University, Seoul 136-701, Republic of Korea*

Hyun Geun Lee‡ and Junseok Kim§

*Department of Mathematics, Korea University, Seoul 136-701, Republic of Korea*

(Received December 19 2008)

## Abstract

Understanding pinchoff in a liquid-liquid jet is one of the fundamental problems in the physics of fluid. Pinchoff has a wide variety of applications such as in ink-jet printers. We have numerically investigated the breakup of a forced liquid jet into drops in immiscible liquid-liquid systems with a phase-field model. In the phase-field model, the classical sharp interface between the two immiscible fluids is represented by a transition region of small but finite width. Across this width the composition of one of the two fluids changes continuously. The phase-field method can deal with topological transitions such as breakup and reconnection smoothly without ad hoc “cut and connect” or smoothing procedures. We compared the numerical results on the pinchoff of liquid-liquid jets with surface tension finding good agreement with experimental data. In particular, we investigated axial velocity and vorticity structures around the jet neck before and after pinchoff.

PACS numbers: 47.10.ad,02.70.Bf,47.11.Bc

Keywords: Liquid jet, pinchoff, Navier-Stokes equation, Cahn-Hilliard equation, finite difference method, projection method, phase-field method

---

\*Electronic address: [chkim@korea.ac.kr](mailto:chkim@korea.ac.kr)

†Electronic address: [winstorm@korea.ac.kr](mailto:winstorm@korea.ac.kr)

‡Electronic address: [leeh@korea.ac.kr](mailto:leeh@korea.ac.kr)

§Electronic address: [cfdkim@korea.ac.kr](mailto:cfdkim@korea.ac.kr); Fax: +82-2-929-8562

## I. INTRODUCTION

Free boundary problems represent excellent approximations to a number of important engineering, industrial, and biomedical problems such as breakup of a liquid column surrounded by another fluid [1]. However, one of the great difficulties in the study of two immiscible fluid flows is the presence of an interface. The interface changes and may undergo severe topological deformations such as breakup and merging.

The phase-field model [2] provides a natural way of capturing the evolution of complex interfaces and treating the topological changes of the interface. In this model, a mass concentration field  $c(\mathbf{x}, t)$  is introduced to denote the mass fraction of one of the components in a heterogeneous mixture of two fluids. The mass concentration is coupled to the fluid motion through concentration dependent density, viscosity, and surface tension force. The resulting system couples the Navier-Stokes equations to a fourth order, degenerate, non-linear parabolic diffusion equation of the Cahn-Hilliard type for the concentration. The advantages of this approach are: (1) Topological changes, such as the interface merging and breakup, can be treated without difficulty. (2) The phase field has physical meanings not only on the interface but also in the bulk phases. Therefore, this method can be applied to many physical applications. (3) It can be straightforwardly extended to a three dimensional multicomponent system. There are other approaches such as the lattice Boltzmann method [3, 4] to study multiphase flow [5]. Anderson, McFadden and Wheeler have authored a review paper of this phase-field model [6].

This paper is organized in the following manner. The definition and formulation of the governing equation in cylindrical coordinates for the solution to the problem of a Newtonian liquid jet injected vertically into another Newtonian quiescent liquid are introduced in Section II. We describe a numerical method in Section III. We compare the numerical experiments with available experimental data from Milosevic and Longmire [1] in Section IV. Finally, we present conclusions in Section V.

## II. PROBLEM DEFINITION AND FORMULATION

In this paper, we consider a liquid-liquid jet that pinches off making droplets. The experimental setup, consisting of a tank, a pump, a control valve, a rotameter, and a forcing

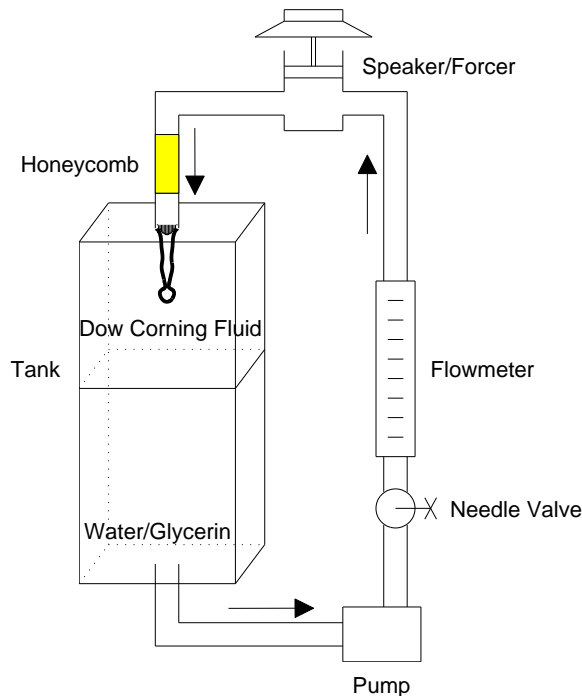


FIG. 1: Recirculating jet facility.

apparatus, is illustrated in Fig. 1. The dimensions of the tank are  $20.3 \times 20.3 \times 56 \text{ cm}^3$ . A magnetic-driven pump generates a steady flow controlled by a needle valve. The flow (a water/glycerin mixture) passes through a honeycomb straightener before exiting a nozzle into an ambient layer of the Dow Corning fluid. More details about the experimental setup are in [1]. The flow configuration, investigated numerically in our study, is shown in Fig. 2. The jet of a viscous fluid 1 is injected vertically from a circular nozzle downwards into a tank of stationary mutually saturated immiscible fluid 2. The viscosity and density of the inner jet fluid 1 are denoted by  $\eta_1$  and  $\rho_1$ , respectively. Likewise, those of the outer ambient fluid 2 are denoted by  $\eta_2$  and  $\rho_2$ , respectively. The domain is axisymmetric with the center line being the axis of symmetry.

### A. The Governing Equations

We consider a situation of a binary fluid consisting of two components, fluid 1 and fluid 2. We denote the composition of component 1, expressed as a mass fraction, by  $c(\mathbf{x}, t)$ , where  $\mathbf{x}$  is space position and  $t$  is time. In this setting the composition plays the role of an order parameter that distinguishes the different phases of the fluid. Then, in dimensional form,

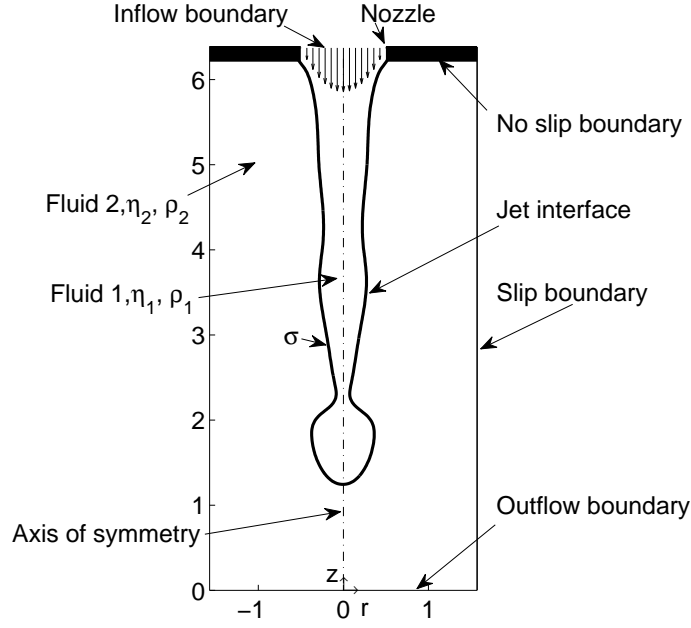


FIG. 2: The liquid/liquid jet flow configuration.

the phase-field model [7] is

$$\nabla \cdot \mathbf{u} = 0, \quad (1)$$

$$\rho \dot{\mathbf{u}} = -\nabla p + \nabla \cdot [\eta(c)(\nabla \mathbf{u} + \nabla \mathbf{u}^T)] - 6\sqrt{2}\epsilon\sigma \nabla \cdot \left( \frac{\nabla c}{|\nabla c|} \right) |\nabla c| \nabla c + \rho \mathbf{g}, \quad (2)$$

$$\dot{c} = \nabla \cdot (M(c)\nabla \mu), \quad (3)$$

$$\mu = f(c) - \epsilon^2 \Delta c, \quad (4)$$

where  $\dot{\cdot} = \partial_t + \mathbf{u} \cdot \nabla$  is the total derivative,  $\mathbf{u}$  is the velocity,  $p$  is the pressure,  $\rho(c) = \rho_1 c + \rho_2(1 - c)$  is the density, and  $\eta(c) = \eta_1 c + \eta_2(1 - c)$  is the viscosity.  $-6\sqrt{2}\epsilon\sigma \nabla \cdot \left( \frac{\nabla c}{|\nabla c|} \right) |\nabla c| \nabla c$  is the interfacial tension body force concentrated on the interface, where  $\sigma$  is the interfacial tension coefficient, and  $\epsilon$  is the interface thickness parameter.  $M(c) = M c(1 - c)$  is the variable mobility,  $\mu$  is the generalized chemical potential, and  $f(c) = F'(c)$ .  $F(c)$  is the Helmholtz free energy where  $F(c) = \frac{1}{4}c^2(1 - c)^2$  (see Fig. 3).

## B. The Nondimensional Governing Equations

The next step is to restate the dimensional phase-field model in dimensionless form. For this purpose, we define characteristic values such as length ( $L_*$ ), velocity ( $V_*$ ), viscosity ( $\eta_*$ ), density ( $\rho_*$ ), chemical potential ( $\mu_*$ ), and mobility ( $M_*$ ). We then introduce non-dimensional variables for the space coordinates, time, the velocity components, viscosity,

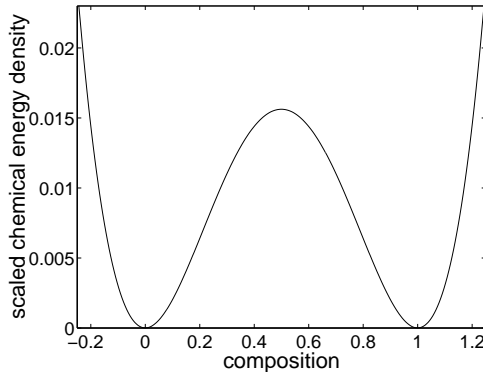


FIG. 3: A double well potential,  $F(c) = 0.25c^2(c - 1)^2$ .

the fluid pressure, interface thickness, chemical potential, and mobility:

$$\bar{x} = \frac{x}{L_*}, \quad \bar{\mathbf{u}} = \frac{\mathbf{u}}{V_*}, \quad \bar{\eta} = \frac{\eta}{\eta_*}, \quad \bar{p} = \frac{p}{\rho_* V_*^2}, \quad \bar{\epsilon} = \frac{\epsilon}{L_*}, \quad \bar{\mu} = \frac{\mu}{\mu_*}, \quad \bar{M} = \frac{M}{M_*},$$

where the bars denote dimensionless variables. Substituting these variables into the governing Eqs. (1)-(4), dropping the bar notations, and using the dimensionless numbers yield the following nondimensional system:

$$\nabla \cdot \mathbf{u} = 0, \tag{5}$$

$$\begin{aligned} \mathbf{u}_t + \mathbf{u} \cdot \nabla \mathbf{u} = & -\nabla p + \frac{1}{Re} \nabla \cdot [\eta(c)(\nabla \mathbf{u} + \nabla \mathbf{u}^T)] \\ & - \frac{6\sqrt{2}\epsilon}{We} \nabla \cdot \left( \frac{\nabla c}{|\nabla c|} \right) |\nabla c| \nabla c + \frac{\rho - 1}{Fr^2} \mathbf{G}, \end{aligned} \tag{6}$$

$$c_t + \mathbf{u} \cdot \nabla c = \frac{1}{Pe} \nabla \cdot (M(c) \nabla \mu), \tag{7}$$

$$\mu = f(c) - \epsilon^2 \Delta c. \tag{8}$$

The dimensionless parameters are the Reynolds number,  $Re = \rho_* V_* L_* / \eta_*$ ; the Weber number,  $We = \rho_* L_* V_*^2 / \sigma$ ; the Froude number,  $Fr = V_* / \sqrt{L_* g}$ ; and the diffusional Peclet number,  $Pe = L_* V_* / (M_* \mu_*)$ .

### C. The Axisymmetric Navier-Stokes Cahn-Hilliard System

In this paper we consider only axisymmetric flows; therefore, there is no flow in the  $\theta$  (azimuthal) direction and all  $\theta$  derivatives are identically zero. Therefore we consider only two variables,  $r$  the radial direction and  $z$  the axial direction in the two-dimensional axisymmetric domain  $\Omega = \{(r, z) : 0 < r < R, 0 < z < H\}$ . We define the fluid velocity by

the vector  $\mathbf{u} = (u, w)$ , where  $u = u(r, z)$  is the radial component of velocity and  $w = w(r, z)$  is the component in the axial direction. We use the Boussinesq approximation to represent the gravitational force due to a density difference between the jet and the ambient fluid. The governing equations for axisymmetric flow are

$$\frac{1}{r}(ru)_r + w_z = 0, \quad (9)$$

$$u_t + uu_r + wu_z = -p_r + \frac{1}{Re} \left[ \frac{1}{r}(r(2\eta u_r))_r + (\eta(w_r + u_z))_z - \frac{2\eta u}{r^2} \right] + F_1, \quad (10)$$

$$w_t + ww_r + ww_z = -p_z + \frac{1}{Re} \left[ \frac{1}{r}(r\eta(w_r + u_z))_r + (2\eta w_z)_z \right] + F_2 - \frac{\rho - 1}{Fr^2}, \quad (11)$$

$$c_t + uc_r + wc_z = \frac{1}{Pe} \left[ \frac{1}{r}(rM(c)\mu_r)_r + (M(c)\mu_z)_z \right], \quad (12)$$

$$\mu = f(c) - \epsilon^2 \left[ \frac{1}{r}(rc_r)_r + c_{zz} \right], \quad (13)$$

where

$$\mathbf{F} = (F_1, F_2) = -\frac{6\sqrt{2}\epsilon}{We} \nabla \cdot \left( \frac{\nabla c}{|\nabla c|} \right) |\nabla c| \nabla c,$$

and

$$\nabla c = (c_r, c_z), \quad \nabla \cdot (\phi, \psi) = \frac{1}{r}(r\phi)_r + \psi_z,$$

where the subscript indexes  $t$ ,  $r$ , and  $z$  refer to differentiation with respect to the variable.

We, next, specify the boundary conditions. The amplitude of the velocity fluctuation is adjusted such that a droplet is pinched off at the same downstream location as in the experiments. For the inflow into the nozzle, we assume time dependent fully developed Poissuille flow:  $u(r, 2\pi, t) = 0$  and  $w(r, 2\pi, t) = V_*(1 + \alpha \cos(2\pi ft))(1 - r^2)$ , where  $\alpha$  and  $f$  are the amplitude and frequency of the velocity fluctuation, respectively. We define the Strouhal number,  $St = fL_*/V_*$ . Outside of the nozzle, no-slip conditions are used:  $u(r, 2\pi, t) = w(r, 2\pi, t) = 0$ . For the axis of symmetry at  $r = 0$ ,  $u(0, z, t) = \frac{\partial w(0, z, t)}{\partial r} = 0$ . For the outflow boundary at the bottom of the mesh,  $z = 0$ . We assume no change in the axial direction:  $\frac{\partial u(r, 0, t)}{\partial z} = \frac{\partial w(r, 0, t)}{\partial z} = 0$ .

### III. THE NUMERICAL METHOD

We employ a Chorin-type projection method for the decoupling of the momentum and continuity equations. Our strategy for solving the system (9)-(13) is a fractional step scheme having two parts. First, we solve the momentum and concentration equations (10)-(11)

without strictly enforcing the incompressibility constraint (9); then, we project the resulting velocity field onto the space of discretely divergence-free vector fields [8]. Then, we update the phase field in Eqs. (12) and (13). We provide a detailed description is described in Appendix A.

#### IV. NUMERICAL EXPERIMENTS

In our numerical simulations, we use the mean value for the flow rate at the nozzle. Then, the simulation follows the time evolution of the flow until the jet length versus time profile reaches a pseudo-steady behavior. The initial concentration field and velocity fields are given by

$$c^0(r, z) = 0.5 \left[ 1 - \tanh \left( \frac{r - 0.5 - 0.05 \cos(z)}{2\sqrt{2}\epsilon} \right) \right],$$

$$u^0(r, z) = w^0(r, z) = 0$$

on a domain,  $\Omega = \{(r, z) | 0 \leq r \leq 0.5\pi \text{ and } 0 \leq z \leq 4\pi\}$ . In this computation we use the following parameters:  $\epsilon = 0.02$ ,  $Re = 58$ ,  $We = 0.016$ ,  $St = 3.5$ , and  $Pe = 100/\epsilon$ .

Sequences of phase-locked images are shown in Fig. 4. We divide one cycle into  $360^\circ$  phases. As the liquid filament is stretched by gravity, a neck forms, elongates and becomes thinner. In the meantime, the lower end of the filament turns into a round drop under capillary forces. The falling drop continues to stretch the thread and eventually the Rayleigh instability leads to a pinchoff of the main drop [9].

The normalized axial velocity ( $w$ ) contours of the forced flow at  $St = 3.5$  and  $Re = 58$  are shown in Fig. 5. The highest contour level is 0 and succeeding levels are decreased by 1. We can see that, before pinchoff ( $\Phi = 60^\circ$  and  $\Phi = 90^\circ$ ), the maximum axial velocity is located approximately at the jet neck. The fluid is thus accelerating into the neck and acting to increase the volume of the drop. After the pinchoff, the maximum velocity still resides inside of the drop ( $\Phi = 120^\circ$  and  $\Phi = 150^\circ$ ).

The normalized vorticity field ( $w_r - u_z$ ) contours of the forced flow at  $St = 3.5$  and  $Re = 58$  are shown in Fig. 6. Solid lines represent positive vorticity. The lowest contour level is 0.05. Succeeding levels are incremented by 0.5. Dotted lines represent negative vorticity. The highest contour level is  $-0.05$ . Succeeding levels are decreased by 0.5. At the phase ( $\Phi = 90^\circ$ ), two opposite signed vorticities around the jet neck develop to act to

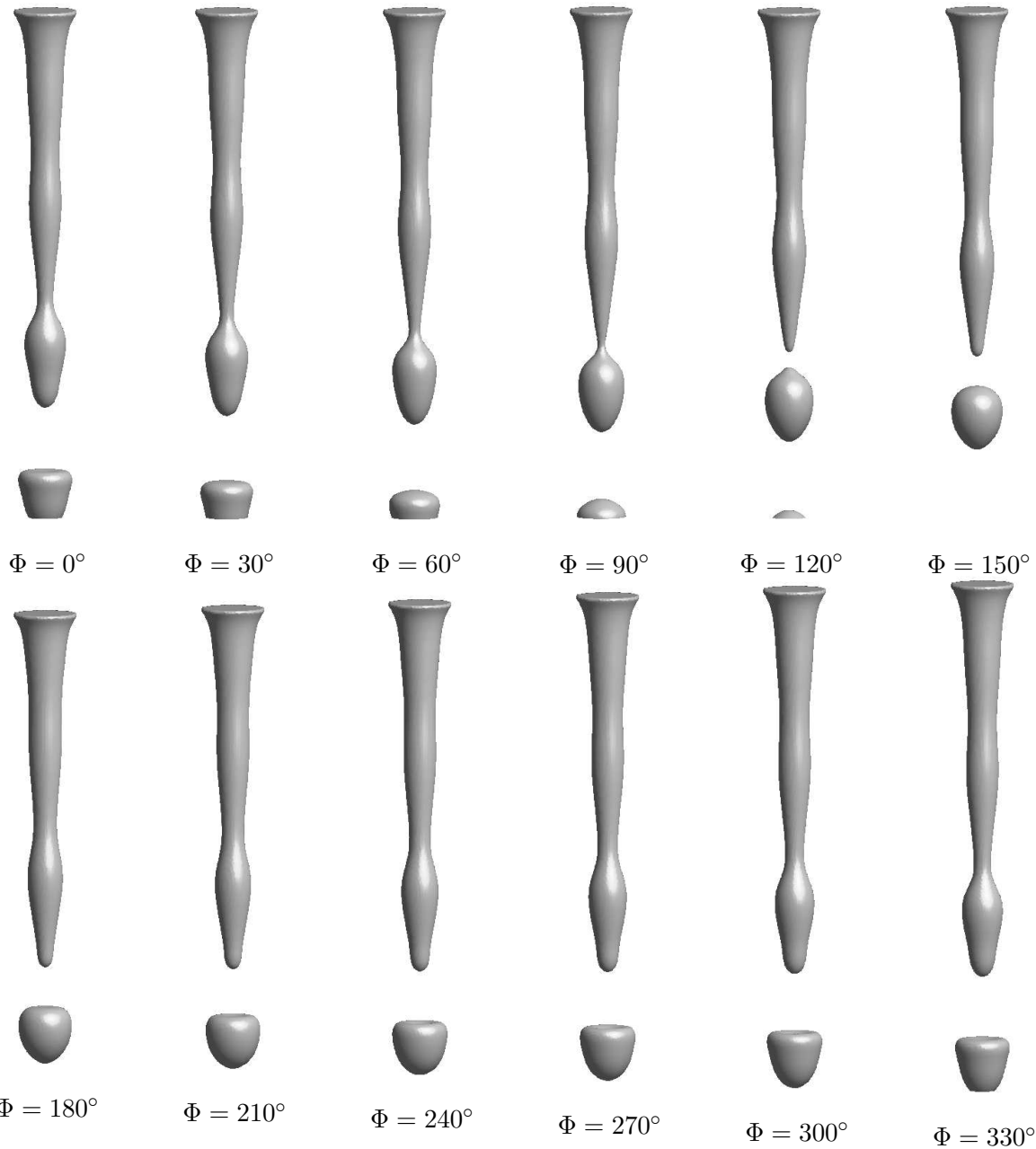


FIG. 4: The time evolution leading to multiple pinchoffs. The phase-locked sequence of jet pinchoff at  $Re = 58$  and  $St = 3.5$ .

encourage pinchoff. The positive vorticity makes the fluid rotate clockwise, while negative vorticity makes the fluid rotate counter-clockwise. After the drop pinches off, a small ring of inverted vorticity develops at the jet tip due to the recoiling interface there.

In Fig. 7, we plot close-up shapes of drops at the phases,  $\Phi = 120^\circ$  and  $\Phi = 240^\circ$ . At  $\Phi = 120^\circ$ , after pinchoff the upstream area of the drop has a large curvature. This curvature and gravity accelerate the axial velocity making a maximum value at the upstream part of



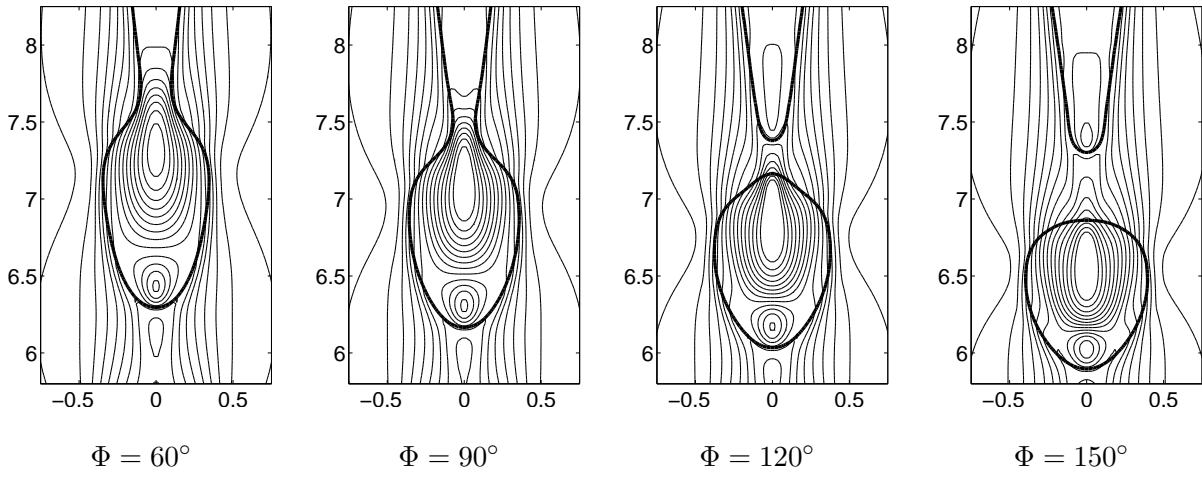


FIG. 5: Normalized axial velocity ( $w$ ) contours of forced flow at  $St = 3.5$  and  $Re = 58$ . The highest contour level is 0. Succeeding levels are decreased by 1.

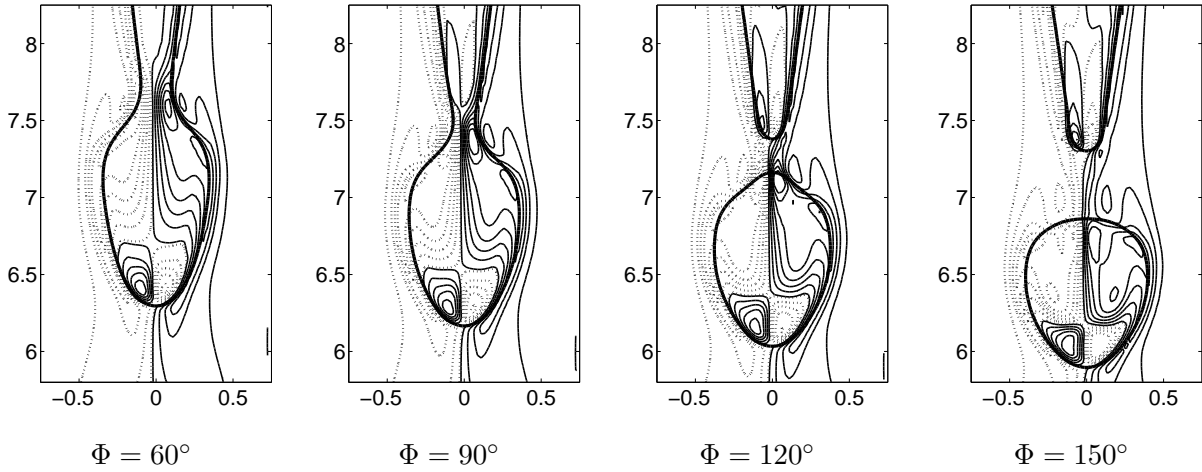


FIG. 6: Normalized vorticity field ( $w_r - u_z$ ) contours of forced flow at  $St = 3.5$  and  $Re = 58$ . The solid lines represent positive vorticity. The lowest contour level is 0.05. Succeeding levels are incremented by 0.5. The dotted lines represent negative vorticity. The highest contour level is  $-0.05$ . Succeeding levels are decreased by 0.5.

the drop. At  $\Phi = 240^\circ$ , the upstream region of the drop has a large dimple. Interfacial tension causes the upstream surface of the drop to recover to a convex shape as the drop falls down. In Fig. 8, (a) and (b) are the normalized axial velocity ( $w$ ) and (c) and (d) are vorticity field ( $w_r - u_z$ ) contours of forced flow. These results are qualitatively in good agreement with the experimental data [1].

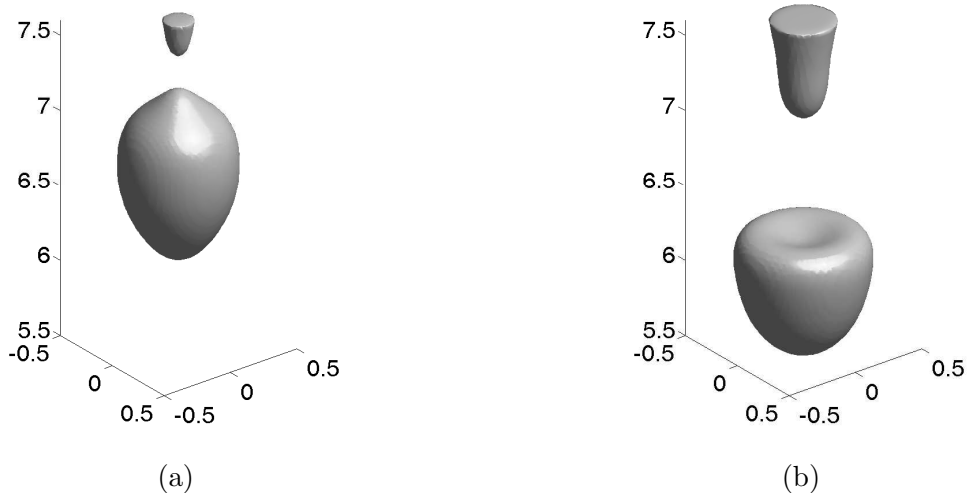


FIG. 7: (a)  $\Phi = 120^\circ$  and (b)  $\Phi = 240^\circ$ .

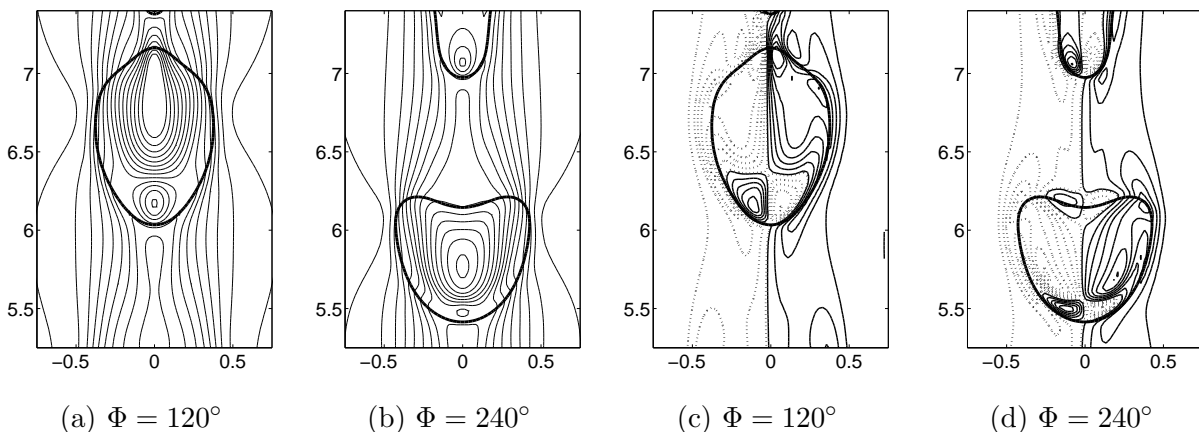


FIG. 8: (a) and (b) are the normalized axial velocity ( $w$ ) and (c) and (d) are the vorticity field ( $w_r - u_z$ ) contours of forced flow.

## V. CONCLUSIONS

In this paper, we described our numerical study of the physics of the pinchoff transition in liquid-liquid jet systems. The numerical method we used is a phase-field model for solving axisymmetric immiscible two-phase flow with variable density, viscosity, surface tension, and gravity. The phase-field model is based on a physical background. It can deal with topological transitions such as jet pinchoff. The axial velocity and vorticity structures around the jet neck before and after pinchoff are qualitatively in good agreement with the experimental results. In the future, we will include an electrostatic field in our governing equations to simulate the electrostatic ejection of liquid droplets [15].

## Acknowledgments

This research was supported by Basic Science Research Program through the National Research Foundation of Korea(NRF) funded by the Ministry of Education, Science and Technology (NO. R01-2008-000-20855-0). The corresponding author (J.S. Kim) was also supported by the MKE(Ministry of Knowledge Economy), Korea, under the ITRC(Information Technology Research Center) support program supervised by the IITA(Institute for Information Technology Advancement) (IITA-2009-C1090-0902-0013). J.S. Kim thanks Professors John Lowengrub, Ellen Longmire, and Dr. Ilja Milosevic for valuable discussions and comments.

## APPENDIX A: THE NUMERICAL PROCEDURE

We use a projection method for solving the system (9)-(13) [8]. The computational grid consists of square cells of size  $h$ ; these cells  $\Omega_{ik}$  are centered at  $(r_i = (i - 0.5)h, z_k = (k - 0.5)h)$ , where  $i = 1, \dots, M$  and  $k = 1, \dots, N$ . The discrete velocity field  $\mathbf{u}_{ik}^n$  and the concentration field  $c_{ik}^n$  are located at the cell centers. The pressure  $p_{i+\frac{1}{2}, k+\frac{1}{2}}^{n-\frac{1}{2}}$  is located at the cell corners. The notation  $\mathbf{u}_{ik}^n$  is used to represent an approximation to  $\mathbf{u}(r_i, z_k, t^n)$ , where  $t^n = n\Delta t$  and  $\Delta t$  is a time step. Given  $\mathbf{u}^{n-1}, \mathbf{u}^n, c^{n-1}, c^n$ , and  $p^{n-\frac{1}{2}}$ , we want to find  $\mathbf{u}^{n+1}, c^{n+1}$ , and  $p^{n+\frac{1}{2}}$  which solve the following equations of motion:

$$\begin{aligned} \nabla_d \cdot \mathbf{u}^{n+1} &= 0, \\ \frac{\mathbf{u}^{n+1} - \mathbf{u}^n}{\Delta t} &= -\nabla_d p^{n+\frac{1}{2}} + \frac{1}{2Re} \nabla_d \cdot \eta(c^{n+1}) [\nabla_d \mathbf{u}^{n+1} + (\nabla_d \mathbf{u}^{n+1})^T] \\ &\quad + \frac{1}{2Re} \nabla_d \cdot \eta(c^n) [\nabla_d \mathbf{u}^n + (\nabla_d \mathbf{u}^n)^T] + \mathbf{F}^{n+\frac{1}{2}} - (\mathbf{u} \cdot \nabla_d \mathbf{u})^{n+\frac{1}{2}}, \\ \frac{c^{n+1} - c^n}{\Delta t} &= \frac{1}{Pe} \nabla_d \cdot (M(c^{n+\frac{1}{2}}) \nabla_d \mu^{n+\frac{1}{2}}) - (\mathbf{u} \cdot \nabla_d c)^{n+\frac{1}{2}}, \end{aligned} \tag{A1}$$

$$\mu^{n+\frac{1}{2}} = \frac{1}{2} [f(c^n) + f(c^{n+1})] - \frac{\epsilon^2}{2} \Delta_d (c^n + c^{n+1}). \tag{A2}$$

The outline of the main procedures in one time step follows:

*Step 1.* Initialize  $c^0$  to be the locally equilibrated concentration profile and  $\mathbf{u}^0$  to be the divergence-free velocity field.

*Step 2.* Update the concentration field  $c^n$  to  $c^{n+1}$ . Details of this step are presented in Section A 1.

*Step 3.* Compute  $(\mathbf{u} \cdot \nabla_d \mathbf{u})^{n+\frac{1}{2}}$  by using a second order ENO (essentially non-oscillatory) scheme. The half time value  $\mathbf{u}_{ik}^{n+\frac{1}{2}}$  is calculated using an extrapolation from previous values. We obtain cell-edged values by  $\mathbf{u}_{i+\frac{1}{2},k}^{n+\frac{1}{2}} = (r_i \mathbf{u}_{ik}^{n+\frac{1}{2}} + r_{i+1} \mathbf{u}_{i+1,k}^{n+\frac{1}{2}})/(2r_{i+\frac{1}{2}})$  and  $\mathbf{u}_{i,k+\frac{1}{2}}^{n+\frac{1}{2}} = (\mathbf{u}_{ik}^{n+\frac{1}{2}} + \mathbf{u}_{i,k+1}^{n+\frac{1}{2}})/2$ . In general, the normal velocities  $u_{i+\frac{1}{2},k}^{n+\frac{1}{2}}$  and  $w_{i,k+\frac{1}{2}}^{n+\frac{1}{2}}$  at the edges are not divergence-free. We apply a MAC projection [10] before constructing the convective derivatives. The equation

$$\Delta_d \phi = \nabla_{MAC} \cdot \mathbf{u}^{n+\frac{1}{2}} \quad (\text{A3})$$

is solved for a cell centered  $\phi$ . We solve the resulting linear system (A3) using a multigrid method with Gauss-Seidel relaxation. Then the divergence-free normal velocities  $\tilde{u}$  and  $\tilde{w}$  are defined by

$$\tilde{u}_{i+\frac{1}{2},k}^{n+\frac{1}{2}} = u_{i+\frac{1}{2},k}^{n+\frac{1}{2}} - \frac{\phi_{i+1,k} - \phi_{ik}}{h}, \quad \tilde{w}_{i,k+\frac{1}{2}}^{n+\frac{1}{2}} = w_{i,k+\frac{1}{2}}^{n+\frac{1}{2}} - \frac{\phi_{i,k+1} - \phi_{ik}}{h}.$$

The convective terms are discretized:

$$\begin{aligned} (\mathbf{u} \cdot \nabla_d \mathbf{u})_{ik}^{n+\frac{1}{2}} &= \frac{r_{i+\frac{1}{2}} \tilde{u}_{i+\frac{1}{2},k} + r_{i-\frac{1}{2}} \tilde{u}_{i-\frac{1}{2},k}}{2r_i h} (\bar{\mathbf{u}}_{i+\frac{1}{2},k} - \bar{\mathbf{u}}_{i-\frac{1}{2},k}) \\ &\quad + \frac{\tilde{w}_{i,k+\frac{1}{2}} + \tilde{w}_{i,k-\frac{1}{2}}}{2h} (\bar{\mathbf{u}}_{i,k+\frac{1}{2}} - \bar{\mathbf{u}}_{i,k-\frac{1}{2}}), \end{aligned}$$

where we suppress the  $n+\frac{1}{2}$  temporal index. The edge values  $\bar{\mathbf{u}}_{i\pm\frac{1}{2},k}^{n+\frac{1}{2}}$  and  $\bar{\mathbf{u}}_{i,k\pm\frac{1}{2}}^{n+\frac{1}{2}}$  are computed using a higher order ENO procedure derived in Ref. [11]. The procedure for computing the quantity  $f_{i+\frac{1}{2},k}$  is:

$$\begin{aligned} j &= \begin{cases} i & \tilde{u}_{i+\frac{1}{2},k} \geq 0 \\ i+1 & \text{otherwise} \end{cases} \\ a &= \frac{f_{jk} - f_{j-1,k}}{h}, \quad b = \frac{f_{j+1,k} - f_{jk}}{h}, \quad d = \begin{cases} a & \text{if } |a| \leq |b| \\ b & \text{otherwise} \end{cases} \\ f_{i+\frac{1}{2},k} &= f_{jk} + \frac{h}{2} d (1 - 2(j-i)). \end{aligned}$$

*Step 4.* We solve

$$\begin{aligned} \frac{\mathbf{u}^* - \mathbf{u}^n}{\Delta t} &= -\nabla_d p^{n-\frac{1}{2}} + \frac{1}{2Re} \nabla_d \cdot \eta(c^{n+1}) [\nabla_d \mathbf{u}^* + (\nabla_d \mathbf{u}^*)^T] \\ &\quad + \frac{1}{2Re} \nabla_d \cdot \eta(c^n) [\nabla_d \mathbf{u}^n + (\nabla_d \mathbf{u}^n)^T] + \mathbf{F}^{n+\frac{1}{2}} - (\mathbf{u} \cdot \nabla_d \mathbf{u})^{n+\frac{1}{2}} \end{aligned} \quad (\text{A4})$$

using a multigrid method for the intermediate velocity  $\mathbf{u}^*$ . Here we use the following discretizations for the derivatives.

$$(\nabla_d p)_{ik} = \begin{pmatrix} \frac{p_{i+\frac{1}{2},k+\frac{1}{2}} + p_{i+\frac{1}{2},k-\frac{1}{2}} - p_{i-\frac{1}{2},k+\frac{1}{2}} - p_{i-\frac{1}{2},k-\frac{1}{2}}}{2h} \\ \frac{p_{i+\frac{1}{2},k+\frac{1}{2}} + p_{i-\frac{1}{2},k+\frac{1}{2}} - p_{i+\frac{1}{2},k-\frac{1}{2}} - p_{i-\frac{1}{2},k-\frac{1}{2}}}{2h} \end{pmatrix}.$$

$$\text{Let } (\mathcal{L}^1, \mathcal{L}^2) = \nabla \cdot [\eta(\nabla \mathbf{u} + \nabla \mathbf{u}^T)] = \begin{pmatrix} \frac{2}{r}(r\eta u_r)_r - \frac{2\eta}{r^2}u + (\eta u_z)_z + (\eta w_r)_z \\ \frac{1}{r}(r\eta u_z)_r + \frac{1}{r}(r\eta w_r)_r + 2(\eta w_z)_z \end{pmatrix}.$$

Then the first component of the viscous terms is discretized as follows:

$$\begin{aligned} \mathcal{L}_{ik}^1 = & \frac{2r_{i+\frac{1}{2}}\eta_{i+\frac{1}{2},k}(u_{i+1,k} - u_{ik}) - 2r_{i-\frac{1}{2}}\eta_{i-\frac{1}{2},k}(u_{ik} - u_{i-1,k})}{r_i h^2} \\ & - \frac{2\eta_{ik}}{r_i^2}u_{ik} + \frac{\eta_{i,k+\frac{1}{2}}(u_{i,k+1} - u_{ik}) - \eta_{i,k-\frac{1}{2}}(u_{ik} - u_{i,k-1})}{h^2} \\ & + \frac{\eta_{i,k+\frac{1}{2}}(w_{i+1,k+1} - w_{i-1,k+1} + w_{i+1,k} - w_{i-1,k})}{4h^2} \\ & - \frac{\eta_{i,k-\frac{1}{2}}(w_{i+1,k} - w_{i-1,k} + w_{i+1,k-1} - w_{i-1,k-1})}{4h^2}, \end{aligned}$$

where  $r_{i+\frac{1}{2}} = (r_{i+1} + r_i)/2$ ,  $\eta_{i+\frac{1}{2},k} = [\eta(c_{ik}) + \eta(c_{i+1,k})]/2$ . Next, we derive a discretization for the surface force term. The vertex-centered normal vector at the top right vertex of cell  $\Omega_{ik}$  is given by

$$\begin{aligned} \mathbf{m}_{i+\frac{1}{2},k+\frac{1}{2}} &= (m_{i+\frac{1}{2},k+\frac{1}{2}}^r, m_{i+\frac{1}{2},k+\frac{1}{2}}^z) \\ &= \left( \frac{c_{i+1,k} + c_{i+1,k+1} - c_{ik} - c_{i,k+1}}{2h}, \frac{c_{i,k+1} + c_{i+1,k+1} - c_{ik} - c_{i+1,k}}{2h} \right). \end{aligned}$$

The curvature is calculated at the cell centers from the vertex-centered normals and is given by

$$\begin{aligned} \kappa(c_{ik}) &= \nabla_d \cdot \left( \frac{\mathbf{m}}{|\mathbf{m}|} \right)_{ik} \\ &= \frac{1}{2h} \left( \frac{\frac{r_{i+\frac{1}{2}}}{r_i} m_{i+\frac{1}{2},k+\frac{1}{2}}^r + m_{i+\frac{1}{2},k+\frac{1}{2}}^z}{|\mathbf{m}_{i+\frac{1}{2},k+\frac{1}{2}}|} + \frac{\frac{r_{i+\frac{1}{2}}}{r_i} m_{i+\frac{1}{2},k-\frac{1}{2}}^r - m_{i+\frac{1}{2},k-\frac{1}{2}}^z}{|\mathbf{m}_{i+\frac{1}{2},k-\frac{1}{2}}|} \right. \\ & \quad \left. - \frac{\frac{r_{i-\frac{1}{2}}}{r_i} m_{i-\frac{1}{2},k+\frac{1}{2}}^r - m_{i-\frac{1}{2},k+\frac{1}{2}}^z}{|\mathbf{m}_{i-\frac{1}{2},k+\frac{1}{2}}|} - \frac{\frac{r_{i-\frac{1}{2}}}{r_i} m_{i-\frac{1}{2},k-\frac{1}{2}}^r + m_{i-\frac{1}{2},k-\frac{1}{2}}^z}{|\mathbf{m}_{i-\frac{1}{2},k-\frac{1}{2}}|} \right). \end{aligned}$$

The cell-centered normal is the average of the vertex normals,

$$\nabla_d c_{ik} = \left( \mathbf{m}_{i+\frac{1}{2},k+\frac{1}{2}} + \mathbf{m}_{i+\frac{1}{2},k-\frac{1}{2}} + \mathbf{m}_{i-\frac{1}{2},k+\frac{1}{2}} + \mathbf{m}_{i-\frac{1}{2},k-\frac{1}{2}} \right) / 4.$$

Therefore, the discretization of the surface tension force formulation  $\mathbf{F}$  is

$$\mathbf{F}(c_{ik}) = -6\sqrt{2}\sigma\epsilon\nabla_d \cdot \left( \frac{\mathbf{m}}{|\mathbf{m}|} \right)_{ik} |\nabla_d c_{ik}| \nabla_d c_{ik}.$$

*Step 5.* Project  $\mathbf{u}^*$  onto the space of discretely divergence-free vector fields and get the velocity  $\mathbf{u}^{n+1}$ , i.e.,  $\mathbf{u}^* = \mathbf{u}^{n+1} + \Delta t \nabla_d \phi$ , where  $\phi$  satisfies  $\Delta_d \phi = \nabla_d \cdot \frac{\mathbf{u}^* - \mathbf{u}^n}{\Delta t}$ .

*Step 6.* Update pressure field,  $p^{n+\frac{1}{2}} = p^{n-\frac{1}{2}} + \phi$ . These steps complete one time step.

## 1. The Numerical Solution of the Axisymmetric Cahn-Hilliard Equation

We use a nonlinear Full Approximation Storage (FAS) multigrid method [12–14] to solve the nonlinear discrete system at the implicit time level. Let us rewrite equations (A1) and (A2) as follows.

$$NSO(c^{n+1}, \mu^{n+\frac{1}{2}}) = (\phi^n, \psi^n),$$

where

$$NSO(c^{n+1}, \mu^{n+\frac{1}{2}}) = \left( \frac{c^{n+1}}{\Delta t} - \frac{1}{Pe} \nabla_d \cdot (M(c)^{n+\frac{1}{2}} \nabla_d \mu^{n+\frac{1}{2}}), \right. \\ \left. \mu^{n+\frac{1}{2}} - \frac{1}{2} f(c^{n+1}) + \frac{\epsilon^2}{2} \Delta_d c^{n+1} \right).$$

The source term is  $(\phi^n, \psi^n) = (\frac{c^n}{\Delta t} + s^{n+\frac{1}{2}}, \frac{1}{2} f(c^n) - \frac{\epsilon^2}{2} \Delta_d c^n)$  where  $s^{n+\frac{1}{2}} = -(\mathbf{u} \cdot \nabla_d c)^{n+\frac{1}{2}}$ .

We assume a sequence of grids  $\Omega_l$  ( $\Omega_{l-1}$  is coarser than  $\Omega_l$  by a factor of 2).

### The FAS multigrid cycle

$$\{c_l^{m+1}, \mu_l^{m+\frac{1}{2}}\} = FAScycle(l, c_l^n, c_l^m, \mu_l^{m-\frac{1}{2}}, NSO_l, \phi_l^n, \psi_l^n, \nu).$$

*Step I)* Presmoothing

Compute  $\{\bar{c}_l^m, \bar{\mu}_l^{m-\frac{1}{2}}\}$  by applying  $\nu$  smoothing steps to  $\{c_l^m, \mu_l^{m-\frac{1}{2}}\}$

$$\{\bar{c}_l^m, \bar{\mu}_l^{m-\frac{1}{2}}\} = SMOOTH^\nu(c_l^n, c_l^m, \mu_l^{m-\frac{1}{2}}, NSO_l, \phi_l^n, \psi_l^n).$$

One *SMOOTH* relaxation operator step consists of solving the system (A7) and (A8) given

below by a  $2 \times 2$  matrix inversion for each  $i$  and  $k$ . Let us discretize Eq. (A1) to get a smooth operator.

$$\begin{aligned}
\frac{c_{ik}^{n+1}}{\Delta t} + \left( \frac{r_{i+\frac{1}{2}} M_{i+\frac{1}{2},k}^{n+\frac{1}{2}} + r_{i-\frac{1}{2}} M_{i-\frac{1}{2},k}^{n+\frac{1}{2}}}{r_i h^2 Pe} + \frac{M_{i,k+\frac{1}{2}}^{n+\frac{1}{2}} + M_{i,k-\frac{1}{2}}^{n+\frac{1}{2}}}{h^2 Pe} \right) \mu_{ik}^{n+\frac{1}{2}} \\
= \frac{c_{ik}^n}{\Delta t} + s_{ik}^{n+\frac{1}{2}} + \frac{r_{i+\frac{1}{2}} M_{i+\frac{1}{2},k}^{n+\frac{1}{2}} \mu_{i+1,k}^{n+\frac{1}{2}} + r_{i-\frac{1}{2}} M_{i-\frac{1}{2},k}^{n+\frac{1}{2}} \mu_{i-1,k}^{n+\frac{1}{2}}}{r_i h^2 Pe} \\
+ \frac{M_{i,k+\frac{1}{2}}^{n+\frac{1}{2}} \mu_{i,k+1}^{n+\frac{1}{2}} + M_{i,k-\frac{1}{2}}^{n+\frac{1}{2}} \mu_{i,k-1}^{n+\frac{1}{2}}}{h^2 Pe}, \tag{A5}
\end{aligned}$$

where  $M_{i+\frac{1}{2},k}^{n+\frac{1}{2}} = M((c_{ik}^{n+1} + c_{i+1,k}^{n+1} + c_{ik}^n + c_{i+1,k}^n)/4)$ . Next, let us discretize Eq. (A2). Since  $f(c_{ik}^{n+1})$  is nonlinear with respect to  $c_{ik}^{n+1}$ , we linearize  $f(c_{ik}^{n+1})$  at  $c_{ik}^m$ , i.e.,  $f(c_{ik}^{n+1}) \approx f(c_{ik}^m) + \frac{df(c_{ik}^m)}{dc} (c_{ik}^{n+1} - c_{ik}^m)$ . After substitution of this into (A2) and rearranging the terms, we get

$$\begin{aligned}
- \left( \frac{df(c_{ik}^m)}{2dc} + \frac{2\epsilon^2}{h^2} \right) c_{ik}^{n+1} + \mu_{ik}^{n+\frac{1}{2}} = \frac{1}{2} f(c_{ik}^n) - \frac{\epsilon^2}{2} \Delta_d c_{ik}^n + \frac{1}{2} f(c_{ik}^m) \\
- \frac{df(c_{ik}^m)}{2dc} c_{ik}^m - \frac{\epsilon^2}{2} \left( \frac{r_{i+\frac{1}{2}} c_{i+1,k}^m + r_{i-\frac{1}{2}} c_{i-1,k}^m}{r_i h^2} + \frac{c_{i,k+1}^m + c_{i,k-1}^m}{h^2} \right). \tag{A6}
\end{aligned}$$

Next, we replace  $c_{jl}^{n+1}$  and  $\mu_{jl}^{n+\frac{1}{2}}$  in Eqs. (A5) and (A6) with  $\bar{c}_{jl}^m$  and  $\bar{\mu}_{jl}^{m-\frac{1}{2}}$  if  $(j < i)$  or  $(j = i \text{ and } l \leq k)$ , otherwise with  $c_{jl}^m$  and  $\mu_{jl}^{m-\frac{1}{2}}$ , i.e.,

$$\begin{aligned}
\frac{\bar{c}_{ik}^m}{\Delta t} + \left( \frac{r_{i+\frac{1}{2}} M_{i+\frac{1}{2},k}^{n+\frac{1}{2}} + r_{i-\frac{1}{2}} M_{i-\frac{1}{2},k}^{n+\frac{1}{2}}}{r_i h^2 Pe} + \frac{M_{i,k+\frac{1}{2}}^{n+\frac{1}{2}} + M_{i,k-\frac{1}{2}}^{n+\frac{1}{2}}}{h^2 Pe} \right) \bar{\mu}_{ik}^{m-\frac{1}{2}} \\
= \frac{c_{ik}^n}{\Delta t} + s_{ik}^{n+\frac{1}{2}} + \frac{r_{i+\frac{1}{2}} M_{i+\frac{1}{2},k}^{n+\frac{1}{2}} \mu_{i+1,k}^{m-\frac{1}{2}} + r_{i-\frac{1}{2}} M_{i-\frac{1}{2},k}^{n+\frac{1}{2}} \mu_{i-1,k}^{m-\frac{1}{2}}}{r_i h^2 Pe} \\
+ \frac{M_{i,k+\frac{1}{2}}^{n+\frac{1}{2}} \mu_{i,k+1}^{m-\frac{1}{2}} + M_{i,k-\frac{1}{2}}^{n+\frac{1}{2}} \mu_{i,k-1}^{m-\frac{1}{2}}}{h^2 Pe}, \tag{A7}
\end{aligned}$$

$$\begin{aligned}
- \left( \frac{df(c_{ik}^m)}{2dc} + \frac{2\epsilon^2}{h^2} \right) \bar{c}_{ik}^m + \bar{\mu}_{ik}^{m-\frac{1}{2}} = \frac{1}{2} f(c_{ik}^n) - \frac{\epsilon^2}{2} \Delta_d c_{ik}^n + \frac{1}{2} f(c_{ik}^m) \\
- \frac{df(c_{ik}^m)}{2dc} c_{ik}^m - \frac{\epsilon^2}{2} \left( \frac{r_{i+\frac{1}{2}} c_{i+1,k}^m + r_{i-\frac{1}{2}} \bar{c}_{i-1,k}^m}{r_i h^2} + \frac{c_{i,k+1}^m + \bar{c}_{i,k-1}^m}{h^2} \right). \tag{A8}
\end{aligned}$$

*Step II*) Compute the defect:  $(\bar{d}_{1l}^m, \bar{d}_{2l}^m) = (\phi_l^n, \psi_l^n) - NSO_l(\bar{c}_l^m, \bar{c}_l^m, \bar{\mu}_l^{m-\frac{1}{2}})$ .

- Restrict the defect and  $\{\bar{c}_l^m, \bar{\mu}_l^{m-\frac{1}{2}}\}$ :

$$(\bar{d}_{1l-1}^m, \bar{d}_{2l-1}^m) = I_l^{l-1}(\bar{d}_{1l}^m, \bar{d}_{2l}^m), \quad (\bar{c}_{l-1}^m, \bar{\mu}_{l-1}^{m-\frac{1}{2}}) = I_l^{l-1}(\bar{c}_l^m, \bar{\mu}_l^{m-\frac{1}{2}}).$$

The restriction operator  $I_l^{l-1}$  maps  $l$ -level functions to  $(l-1)$ -level functions.

$$\begin{aligned} c_{l-1}(r_i, z_k) &= I_l^{l-1}c_l(r_i, z_k) = \frac{1}{4h^2r_i} \int_{z_{k-1}}^{z_{k+1}} \int_{r_{i-1}}^{r_{i+1}} c(r, z) r dr dz \\ &= [r_{i-\frac{1}{2}}(c_{i-\frac{1}{2}, k-\frac{1}{2}} + c_{i-\frac{1}{2}, k+\frac{1}{2}}) + r_{i+\frac{1}{2}}(c_{i+\frac{1}{2}, k-\frac{1}{2}} + c_{i+\frac{1}{2}, k+\frac{1}{2}})] / (4r_i) \end{aligned}$$

- Compute the right-hand side:

$$(\phi_{l-1}^n, \psi_{l-1}^n) = (\bar{d}_{1l-1}^m, \bar{d}_{2l-1}^m) + NSO_{l-1}(\bar{c}_{l-1}^n, \bar{c}_{l-1}^m, \bar{\mu}_{l-1}^{m-\frac{1}{2}}).$$

- Compute an approximate solution  $\{\hat{c}_{l-1}^m, \hat{\mu}_{l-1}^{m-\frac{1}{2}}\}$  of the coarse grid equation on  $\Omega_{l-1}$ , i.e.

$$NSO_{l-1}(c_{l-1}^n, c_{l-1}^m, \mu_{l-1}^{m-\frac{1}{2}}) = (\phi_{l-1}^n, \psi_{l-1}^n). \quad (\text{A9})$$

If  $l = 1$ , we employ smoothing steps. If  $l > 1$ , we solve (A9) by performing a FAS  $l$ -grid cycle using  $\{\bar{c}_{l-1}^m, \bar{\mu}_{l-1}^{m-\frac{1}{2}}\}$  as an initial approximation:

$$\{\hat{c}_{l-1}^m, \hat{\mu}_{l-1}^{m-\frac{1}{2}}\} = \text{FAScycle}(l-1, c_{l-1}^n, \bar{c}_{l-1}^m, \bar{\mu}_{l-1}^{m-\frac{1}{2}}, NSO_{l-1}, \phi_{l-1}^n, \psi_{l-1}^n, \nu).$$

- Compute the coarse grid correction (CGC):

$$\hat{v}_{1l-1}^m = \hat{c}_{l-1}^m - \bar{c}_{l-1}^m, \quad \hat{v}_{2l-1}^{m-\frac{1}{2}} = \hat{\mu}_{l-1}^{m-\frac{1}{2}} - \bar{\mu}_{l-1}^{m-\frac{1}{2}}.$$

- Interpolate the correction:  $\hat{v}_{1l}^m = I_{l-1}^l \hat{v}_{1l-1}^m$ ,  $\hat{v}_{2l}^{m-\frac{1}{2}} = I_{l-1}^l \hat{v}_{2l-1}^{m-\frac{1}{2}}$ . The interpolation operator  $I_{l-1}^l$  maps  $(l-1)$ -level functions to  $l$ -level functions. Then the prolongation operator  $I_{l-1}^l$  from  $\Omega_{l-1}$  to  $\Omega_l$  is defined by

$$\begin{pmatrix} v_l(r_{i-\frac{1}{2}}, z_{k-\frac{1}{2}}) \\ v_l(r_{i-\frac{1}{2}}, z_{k+\frac{1}{2}}) \\ v_l(r_{i+\frac{1}{2}}, z_{k-\frac{1}{2}}) \\ v_l(r_{i+\frac{1}{2}}, z_{k+\frac{1}{2}}) \end{pmatrix} = v_{l-1}(r_i, z_k) \begin{pmatrix} \frac{r_i}{r_{i-\frac{1}{2}}} \\ \frac{r_i}{r_{i-\frac{1}{2}}} \\ \frac{r_i}{r_{i+\frac{1}{2}}} \\ \frac{r_i}{r_{i+\frac{1}{2}}} \end{pmatrix}.$$



- Compute the corrected approximation on  $\Omega_l$

$$c_l^m, \text{ after } CGC = \bar{c}_l^m + \hat{v}_{1l}^m, \quad \mu_l^{m-\frac{1}{2}}, \text{ after } CGC = \bar{\mu}_l^{m-\frac{1}{2}} + \hat{v}_{2l}^{m-\frac{1}{2}}.$$

*Step III*) Postsmoothing: Compute  $\{c_l^{m+1}, \mu_l^{m+\frac{1}{2}}\}$  by applying  $\nu$  smoothing steps to  $c_l^m, \text{ after } CGC, \mu_l^{m-\frac{1}{2}}, \text{ after } CGC$ .

$$\{c_l^{m+1}, \mu_l^{m+\frac{1}{2}}\} = SMOOTH^\nu(c_l^n, c_l^m, \text{ after } CGC, \mu_l^{m-\frac{1}{2}}, \text{ after } CGC, NSO_l, \phi_l^n, \psi_l^n).$$

This completes the description of a nonlinear FAScycle for the axisymmetric Cahn-Hilliard equation.

- 
- [1] I. N. Milosevic and E. K. Longmire, *Int. J. Multiphase Flow* **28**, 1853 (2002).
  - [2] J. S. Lowengrub and L. Truskinovsky, *Proc. R. Soc. Lond. A* **454**, 2617 (1998).
  - [3] J. S. Maeng, K. S. Yoo, S. Song, and S. Heu, *J. Korean Phys. Soc.* **48**, 902 (2006).
  - [4] S. J. An, Y. D. Kim, S. Heu, and J. S. Maeng, *J. Korean Phys. Soc.* **49**, 651 (2006).
  - [5] R. Zhang, X. He, and S. Chen, *Comput. Phys. Commun.* **129**, 121 (2000).
  - [6] D. M. Anderson, G. B. McFadden, and A. A. Wheeler, *Ann. Rev. Fluid Mech.* **30**, 139 (1998).
  - [7] J. S. Kim, *J. Comput. Phys.* **204**, 784 (2005).
  - [8] J. B. Bell, P. Collela, and H. M. Glaz, *J. Comput. Phys.* **85**, 257 (1989).
  - [9] X. Yang, J. J. Feng, C. Liu, and J. Shen, *J. Comput. Phys.* **218**, 417 (2006).
  - [10] M. Sussman and E. G. Puckett, *J. Comput. Phys.* **162**, 301 (2000).
  - [11] C. W. Shu and S. Osher, *J. Comput. Phys.* **83**, 32 (1989).
  - [12] J. S. Kim and H. O. Bae, *J. Korean Phys. Soc.* **53**, 672 (2008).
  - [13] J. S. Kim, *J. Korean Phys. Soc.* **49**, 1903 (2006).
  - [14] U. Trottenberg, C. Oosterlee, and A. Schüller, *MULTIGRID* (Academic press, 2001).
  - [15] Y. J. Kim, H. S. Ko, S. H. Lee, S. U. Son, D. W. Jung, and D. Y. Byun, *J. Korean Phys. Soc.* **51**, S42 (2007).